Computers and Fluids 285 (2024) 106452

Contents lists available at ScienceDirect

Computers and Fluids

journal homepage: www.elsevier.com/locate/compfluid

Effects of two-dimensional reed oscillation on airflow and sound generation in a single-reed instrument

Tsukasa Yoshinaga [a,*], Reo Baba [b], Hiroshi Yokoyama [c], Tetsuro Shoji [b], Akira Miki [b], Akiyoshi Iida [c]

[a] Graduate School of Engineering Science, Osaka University, Toyonaka, Osaka, 560-8531, Japan
[b] Yamaha Corporation, Hamamatsu, Shizuoka, 430-8650, Japan
[c] Toyohashi University of Technology, Toyohashi, Aichi, 441-8580, Japan

ARTICLE INFO

Keywords:
Woodwind instruments
Compressible flow
Reed oscillation
Fluid-structure interaction

ABSTRACT

While two-dimensional (2D) reed oscillation modes of single-reed woodwind instruments have been reported in previous studies, little is known about their effects on airflow and sound generation. In this study, we conducted aeroacoustic simulations of a clarinet mouthpiece and resonator coupled with one-dimensional (1D) and 2D reed deformation models and investigated the changes in flow and sound generation due to the 2D reed vibration. The 1D and 2D reeds were modeled using 1D beam and thin plate theories, respectively, whereas the three-dimensional airflow was simulated by solving the compressible Navier–Stokes equations. The self-sustained oscillations of the 2D reed model mainly exhibited a flexural mode at the fundamental frequency, which is consistent with previous observations. Complex torsional modes were observed only at higher harmonic frequencies. A comparison between the 1D and 2D reed models demonstrated that the 2D reed opened later at the side face of the mouthpiece than the 1D reed owing to the torsional mode, which changed the time variation of the flow rate into the mouthpiece and the far-field sound in the high-frequency range. These results suggest the importance of the torsional deformation characteristics of reeds on the timbre of single-reed instruments.

1. Introduction

The single-reed woodwind instrument produces sound by blowing air through a gap between a reed and mouthpiece. When the sound is produced in the instrument, the reed oscillates with fluctuations of airflow and pressure at the mouthpiece, and the acoustic resonance inside the instrument also affects the reed oscillation. The instrument player controls the mouth pressure and lip forces to modify the reed oscillation, and these relationships have been investigated using artificial blowing machines that mimic players' mouth conditions, e.g., [1-5].

Among the fluid-structure-acoustic interactions in the instrument, the reed structure has been described as a multimode vibrating system [6], and its oscillation characteristics have been examined in previous studies. Two-dimensional (2D) vibration modes of the reed were observed under acoustic excitation, and the relationships between the musical quality of the reed and the flexural and torsional modes were discussed [7]. In addition, using the observed vibration modes, the mechanical parameters of the clarinet reeds were estimated using numerical simulations [8].

Meanwhile, 2D reed modes were observed under self-sustained oscillation conditions using an artificial blower [9-10], and the reed displacement consisted mostly of the first flexural mode, which largely differed from the acoustically excited free vibration modes of [7]. Ukshini and Dirckx [10] indicated that a single-point measurement of the reed tip can provide a good indication of the 2D vibration amplitude.

In addition to mechanical experiments, numerical flow simulations have been applied to various clarinet-like geometries to further investigate the relationship between the players' conditions and the physical phenomena inside the instrument, e.g., [11-16]. In most fluid–structure interaction simulations, the reed oscillation is modeled by the one-dimensional (1D) dynamic Euler–Bernoulli beam theory [17]. Hence, the 2D torsional oscillation modes were neglected in previous flow simulations. Although vibration simulations of a two-dimensional reed model have been conducted under forced oscillation [18-19], to the best of author's knowledge, there has been no attempt to implement the 2D reed oscillation model to a three-dimensional airflow simulation.

* Corresponding author.
E-mail address: yoshinaga.tsukasa.es@osaka-u.ac.jp (T. Yoshinaga).

https://doi.org/10.1016/j.compfluid.2024.106452
Received 11 July 2024; Received in revised form 21 September 2024; Accepted 5 October 2024
Available online 17 October 2024

As it has been demonstrated that the 2D oscillation characteristics of reeds are changed in higher frequency ranges by the individual reed [7] and mouthpiece geometry [10], the influence on the three-dimensional airflow and its sound generation in the instrument caused by the change of the 1D beam model to the 2D plate model in the numerical simulation is of great interest.

Therefore, in this study, we conducted aeroacoustic simulations of a single-reed instrument coupled with 1D and 2D reed deformation models to clarify the effects of two-dimensional reed oscillation on airflow and sound generation. A mechanical experiment using an artificial blower was conducted, and the computational accuracy of the reed-opening waveforms and generated sounds was evaluated. Subsequently, the reed displacement, airflow, and sound generation in the 2D reed model were compared with those in the 1D reed model. This comparison between the 1D and 2D reed models enables us to purely observe the effects of torsional modes of reed deformation that are difficult to control in the experimental setup.

2. Materials and methods

2.1. Numerical simulation

The target musical instrument is a clarinet mouthpiece (4C, Yamaha, Hamamatsu, Japan) connected to a simple resonator called Saxonett (JRS700, Jupiter, Taipei, Taiwan). We simulated an artificial plastic reed (B♭clarinet traditional, hardness M, Forestone, Osaka, Japan) used in the experiment (see section II. B). The resonator has a recorder-like straight cylinder with an inner diameter of 13.3 mm, and all the tone holes were covered. The total length from the mouthpiece tip to the resonator outlet is 307 mm, and the resulting tone becomes C4 (approximately 262 Hz). A pressure chamber with dimensions of 70 × 40 × 43 mm^3 was put at the front of the mouthpiece, as depicted in Fig. 1, to simulate the artificial blower used in the experiment. An inflow region with a constant pressure $p_{in} = 5.5$ kPa and velocity with a flow rate of 157 cm^3/s was set in the chamber. In this study, the axis x is set in the longitudinal direction of the instrument; y denoted the vertical axis; and the axis z is directed to the spanwise direction of the reed. The origin of the coordinate system was set at the center of the mouthpiece tip.

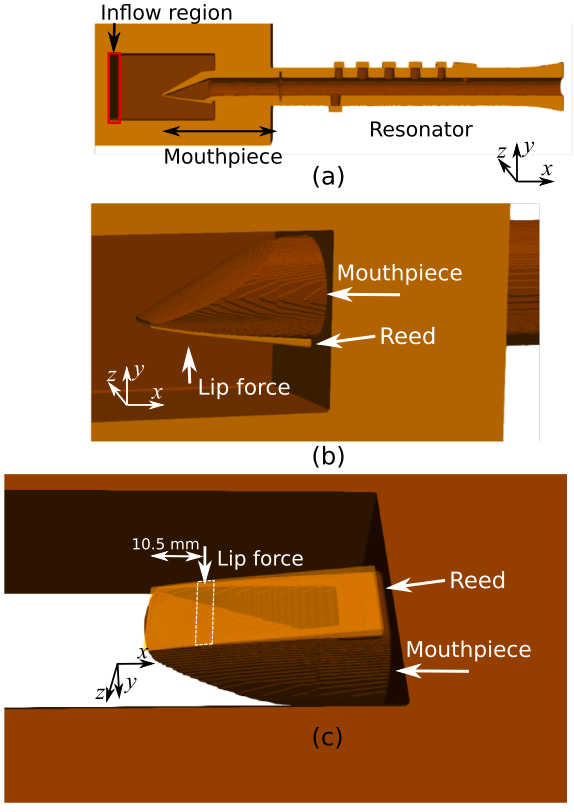

Fig. 1. Instrument geometry for numerical simulation. (a) Center plane of the instrument; (b) close-up view of the mouthpiece; (c) bottom view of the reed and mouthpiece.

The simulation methods for airflow and sound generation are the same as those used in our previous study [16]. The airflow and pressure are calculated by solving the three-dimensional compressible Navier–Stokes equations using the finite-difference method. The spatial derivatives are discretized using the sixth-order accuracy compact scheme [20], whereas time integration is realized using the third-order accuracy Runge–Kutta method. The higher-order schemes enabled the capture of small acoustic pressure fluctuations in large aerodynamic pressures. The moving boundary of the reed part in the structured grids is expressed using the volume penalization (VP) method [21], which is one of the immersed boundary methods. The penalization term, $\mathbf{V}$, is added to right-hand side of the Navier-Stokes equations as,

$$\mathbf{Q}_t + (\mathbf{E} - \mathbf{E}_v)_x + (\mathbf{F} - \mathbf{F}_v)_y + (\mathbf{G} - \mathbf{G}_v)_z = \mathbf{V}, \tag{1}$$

$$\mathbf{V} = -(1/\phi - 1)\chi \begin{pmatrix} \partial \rho u_i / \partial x_i \\ 0 \\ 0 \\ 0 \\ 0 \end{pmatrix}, \tag{2}$$

$$\chi = \begin{cases} \min(1,\ |d/\Delta y|) \\ 0 \end{cases}, \tag{3}$$

where $\mathbf{Q}$ is the vector of the conservative variables, $\mathbf{E}$, $\mathbf{F}$, and $\mathbf{G}$ are inviscid flux vectors, $\mathbf{E}_v$, $\mathbf{F}_v$, and $\mathbf{G}_v$ are viscous flux vectors. The porosity of a porous medium ϕ is determined as $\phi = 0.25$ so that the sound wave can be reflected almost completely (reflectivity: 99 %). The mask function χ is calculated as a function proportional to the distance d between the surface of the moving wall and the closest grid next to it, divided by grid size Δy. A large eddy simulation (LES) was employed using a 10th-order accuracy spatial filter [22] as an implicit turbulence model.

For the 1D reed model, the deformation of the reed structure is described using 1D dynamic beam theory:

$$\rho b h(x)\left[\frac{\partial^2 w(x,t)}{\partial t^2} + \gamma \frac{\partial w(x,t)}{\partial t}\right] + \frac{\partial^2}{\partial x^2}\left[EI(x)\left(1 + \eta \frac{\partial}{\partial t}\right)\frac{\partial^2 w(x,t)}{\partial x^2}\right] = F(x,t), \tag{4}$$

where ρ is the density of the reed, b is the reed width, $h(x)$ is the reed thickness, $w(x,t)$ is a reed displacement, γ is the damping coefficient, E is the Young's modulus, and η is the viscoelastic constant. $I(x)$ is the second moment of area and is calculated as $I(x) = bh(x)^3/12$. The external forces per unit length $F(x,t)$ consist of the fluid, contact, and lip forces, in the same manner as in [17]. The fluid force per unit length was calculated by integrating the acoustic pressure on the reed surface along the z-axis.

When the reed is deformed in 2D, the deformation of a thin isotropic plate with variable thickness in the x-direction can be described as follows [23]:

$$\begin{aligned} &\rho h(x)\left[\frac{\partial^2 w(x,z,t)}{\partial t^2} + \gamma \frac{\partial w(x,z,t)}{\partial t}\right] + \frac{\partial^2}{\partial x^2}\left[D(x)\left(1 + \eta \frac{\partial}{\partial t}\right)\right]\frac{\partial^2 w(x,z,t)}{\partial x^2} \\ &+ 2\frac{\partial^2}{\partial x \partial z}\left[D(x)\left(1 + \eta \frac{\partial}{\partial t}\right)\right]\frac{\partial^2 w(x,z,t)}{\partial x \partial z} + \left[D(x)\left(1 + \eta \frac{\partial}{\partial t}\right)\right]\frac{\partial^4 w(x,z,t)}{\partial z^4} \\ &= F(x,z,t), \end{aligned} \tag{5}$$

where $D(x)$ is calculated as

$$D(x) = \frac{Eh(x)^3}{12(1-\nu^2)}, \tag{6}$$

with a Poisson's ratio ν. $F(x, z, t)$ is the external forces per unit area and is equivalent to the pressure. The external forces of the 2D reed also consist of fluid, contact, and lip forces. Both the 1D and 2D reed deformations are calculated using the finite-difference method. The spatial derivatives are calculated with the 2nd-order accuracy central difference scheme, whereas the time integration is performed using the implicit θ-scheme [17].

The material constants used in the 1D and 2D models are listed in Table 1. The reed density, Young's modulus, and Poisson's ratio were determined based on the material used for the plastic reeds in the experiment [24-25]. Although the reed material consists of polypropylene and cellulose fibers, the fibers are quite short, and we confirmed that there is no difference in Young's moduli in the orthogonal directions. Hence, the material anisotropy (e.g., the change in Young's modulus in the x- and z-directions) was not considered. The viscoelastic constant η for the 2D model was set to zero. The deformable part of the reed ($L \times b = 34 \times 13$ mm^2) was divided into 20 grids along the x-axis in 1D, whereas the 2D reed model was calculated using 24×9 grids in the x-z plane, as shown in Fig. 2. The dependence of grid resolutions of the reed models was checked by reducing the grid sizes, and we confirmed the reed displacement waveforms were almost identical with the finer grids. As the boundary conditions, the reed is clamped at one end ($x = L$) and free at the other end ($x = 0$). For the 2D reed, the reed's side edges ($z = -6.5$ and 6.5) are set to free, and the corner was treated as reported in [19,26].

The contact model was adopted from the penalty method of [17]. While the contact force was considered at all grid points in the 1D model, the contact force in the 2D model was considered only for reed edges where the reed contacted the mouthpiece edges, as depicted in Fig. 2. A contact force was applied to the edges of the 2D reed model when the reed reached the position of the mouthpiece face, whereas the middle of the reed plate was concave inward to the mouthpiece. The reed thickness was set in the same way as in [16] using the following polynomial equation:

$$h(x) = -1.27 \times 10^{-6}x^4 + 8.00 \times 10^{-5}x^3 - 5.99 \times 10^{-4}x^2 + 3.15 \times 10^{-2}x + 0.095. \tag{7}$$

The thickness variation in the z-axis of the 2D reed model were not considered to purely compare the changes between the 1D and 2D models. Moreover, the rounding of the two corner tips of the actual reed was neglected because the 1D model could not consider it.

The lip force per unit length or unit area F_{lip} is modeled as a linear function:

$$F_{lip} = \begin{cases} K_{\mathrm{lip}}\left(w - y_{\mathrm{lip}}\right), & x \in \left[x_{\mathrm{lip}} - L_{\mathrm{lip}},\ x_{\mathrm{lip}} + L_{\mathrm{lip}}\right],\ z \in \left[-b/2,\ b/2\right] \\ 0, & \text{otherwise} \end{cases}, \tag{8}$$

where K_{lip} is the lip stiffness; $2L_{\mathrm{lip}}$ is the lip length; and y_{lip} and x_{lip} are the vertical and spanwise positions of the lip, respectively. The lip force is uniform along the z-direction in the 2D model. The lip position and lip length were kept constant to $y_{\mathrm{lip}} = -7.7$ mm, $x_{\mathrm{lip}} = 11.5$ mm, and $2L_{\mathrm{lip}} = 5.0$ mm in the 1D and 2D models. The lip stiffness was set to $K_{\mathrm{lip}} = 1.7 \times 10^5$ N/m^2 in the 1D model to $K_{\mathrm{lip}} = 6.6 \times 10^6$ N/m^3 in the 2D model to reproduce the lip force measured in the mechanical experiment (0.4 N). Additional lip damping, which is often implemented by increasing γ only at the lip part [15,17,18] was not considered in this simulation because there was little change in the reed deformation waveforms during the preliminary simulations (see Appendix A).

Table 1
Material constants for reed deformation simulation.

	1D reed	2D reed
Reed density ρ (kg/m3)	1140 [24]	1140 [24]
Young's modulus E (GPa)	5.5 [24]	5.5 [24]
Poisson ratio ν (-)	–	0.3 [25]
Damping coefficient γ (1/s)	4000	4000
Viscoelastic constant η (s)	0.6×10^{-6}	0

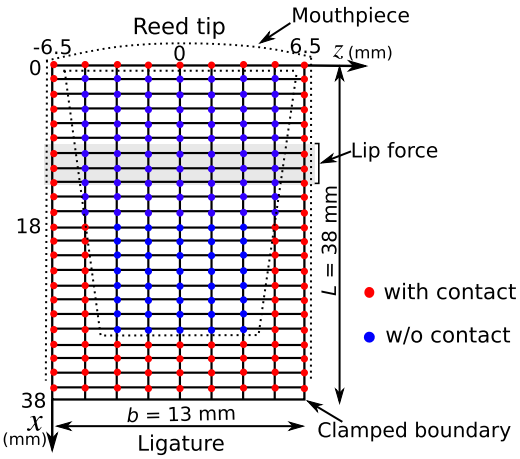

Fig. 2. Positions of 2D reed plate model where contact force of the mouthpiece is applied. The dotted lines indicate the bottom view of the mouthpiece, and the gray bar shows the lip position.

For the fluid and acoustic simulations, the structured computational grids with an approximate total number of 172 million were constructed. The minimum grid size around the reed tip was set to 0.025 mm. The grid size around the sound sampling point was 7.85 mm, indicating that the simulation captured acoustic waves of up to around 6 kHz with eight points per wavelength. The dependency of grid resolution was checked by utilizing a finer grid, where the grid resolution near the instrument was twice as fine as the present values, and the acoustic results were almost identical [14]. The time step of the time integration was set to 2.68×10^{-8} s in both fluid and structural simulations. This value was chosen to resolve the sound propagation of compressible flow in the computational grids. At each time step, the fluid forces on the reed models were calculated from the acoustic pressure, and the reed velocity and displacement were predicted using Eq. (4) and (5). The predicted velocity and displacement of the reed were imposed on the fluid simulation to calculate the flow field in the next time step. The mouth pressure was fixed to $p_{\mathrm{in}} = 5.5$ kPa, which is a typical value for clarinet players [4]. The flow and sound in the initial three cycles of the reed oscillation were simulated without the lip force to obtain a stable self-sustained oscillation. The far-field sound pressure was sampled at 100 mm from the resonator outlet after obtaining a stable oscillation (after the initial six oscillation cycles). The flow simulation was conducted under ideal gas with a room temperature of the experiment (24.6 °C).

2.2. Experimental setups

Mechanical experiments were conducted using an artificial blower to confirm the computational accuracy of the 1D and 2D reed models. The artificial blower shown in Fig. 3 was used to produce sound in the instrument with a mouth pressure of $p_{\mathrm{in}} = 5.5$ kPa. The artificial blower had an inner volume of 90 cm^3, and air was supplied from a compressor (SLP-15, Anest-Iwata, Japan) through a flow meter (PFM750, SMC, Japan) and pressure valve (Model 10,213, Fairchild, NC, USA). The

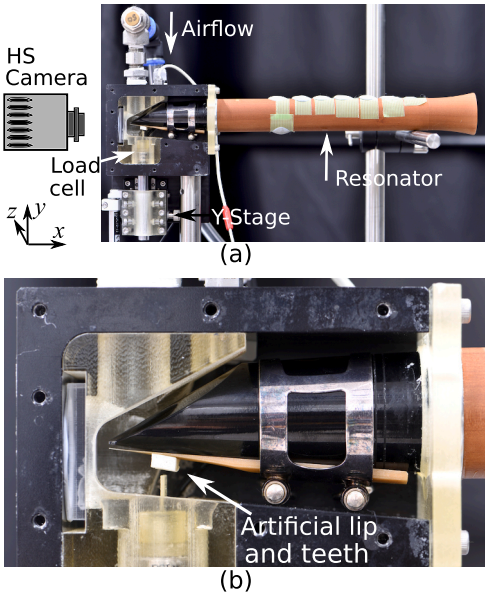

Fig. 3. Experimental setups. (a) Overall experimental equipment; (b) close-up view of the mouthpiece.

pressure inside the blower was measured using a pressure sensor (Model8510B-5, Endevco, NC, USA). The artificial plastic reed (B♭ Clarinet Traditional, Strength M, Forestone, Japan) was set on the mouthpiece with a ligature. The lip force was added by pushing an artificial lip made of a urethane resin ($6 \times 3 \times 14$ mm^3; H0–3K, EXSEAL Co., Ltd., Japan) with a teeth-like plastic blade (thickness of 1 mm) at 11.5 mm from the mouthpiece tip, as shown in Fig. 3(b). The tooth height was adjusted using an X-Y stage, and the force was measured using a load cell (LMU-50, IMADA Co., Ltd., Japan) set between the stage and teeth.

During the measurement, the flow valve and lip height were adjusted to maintain the pressure inside of the artificial blower, and stable oscillations were obtained under the lip forces of 0.40 N and volume flow rates of 157 cm^3/s. The reed-opening waveforms were measured by recording tip movement using a high-speed camera (FASTCAM mini AX200, Photron, Japan) at 6400 fps. The effect of the frame rates on the measurement accuracy is validated in Appendix B. The sound pressure was recorded using a microphone (MI-1271; Onosokki, Japan) at 100 mm from the resonator outlet with a sampling frequency of 51,200 Hz. The room temperature was 24.6 ± 0.2 °C during the experiment.

3. Results

3.1. Comparison with the experiment

The reed-tip opening waveforms of the 1D and 2D models and the experiment are shown in Fig. 4. The reed opening h_r is defined as the distance between the mouthpiece and the reed face, and 0 indicates complete closure. The time $t = 0$ is set at the timing of reed closure. The displacements for the 2D model and experiment were measured at the center of the reed in the z-direction ($z = 0$). The time was normalized by the period of one cycle, which occurred at 258.7, 262.6 and 266.7 Hz for the 1D and 2D models and the experiment, respectively. The waveforms of 1D and 2D models showed an opening phase at $t/T = 0.5$ and a maximum opening of 0.7 mm, whereas the opening phase and maximum opening of the experiment were approximately $t/T = 0.6$ and 0.5 mm, respectively. At this time, the lip forces in the experiment and simulations were 0.4 N.

The sound pressures measured at 100 mm from the resonator outlet in the simulations and experiments are shown in Fig. 5. The overall waveforms of the sound pressure in the simulations were consistent with

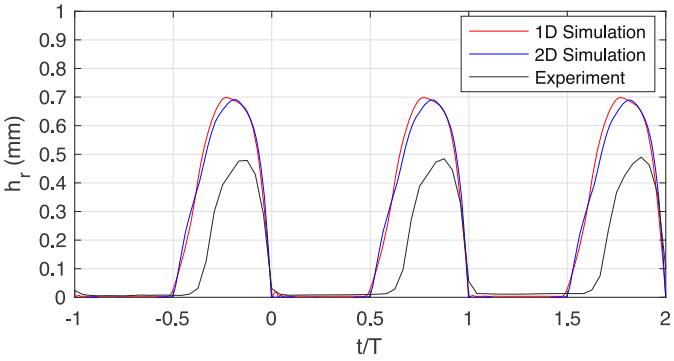

Fig. 4. Reed tip opening h_r of 1D and 2D reed models in simulations and mechanical experiment measured with the high-speed camera.

those in the experiment. These results indicate that although the reed tip waveform was overestimated by both 1D and 2D reed models, aeroacoustic simulations coupled with the reed deformation models can reproduce the physical phenomena inside the instrument and are capable of capturing acoustic characteristics. Although the reed tip waveforms of the 1D and 2D reed models were similar under the same lip force, the detailed pressure waveforms were slightly different. The causes of these differences between the 1D and 2D models are discussed in the following sections.

3.2. Reed deformations

The reed openings in the middle of the reed at $x = 6.7$ mm for the 1D and 2D models are compared in Fig. 6. For the 1D model, the middle of the reed started opening at $t/T = 0.43$ and reached the maximum opening of 0.30 mm. The waveforms were similar to those of the tip opening (Fig. 4). For the 2D model, both the center ($z = 0$) and edge ($z = 6.6$ mm) of the reed had an opening of approximately 0.23 mm and only the center was concaved inward by 0.19 mm during the closed phase. Because the center of the reed was concaved, although the displacement of the center started to increase at $t/T = 0.43$, the reed opening at the edge was at $t/T = 0.50$ and was later than that in the 1D model. In addition, the maximum opening of the 2D model was 0.07 mm smaller than that of the 1D model.

The displacement magnitudes at the fundamental frequency f_0 and

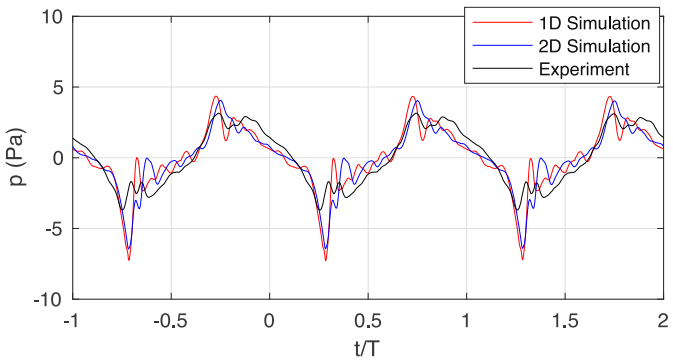

Fig. 5. Sound pressure waveforms measured at 100 mm from the resonator outlet in simulations and experiment.

its harmonics f_1–f_9 for the 2D reed model were calculated using the discretized Fourier Transform (DFT) at each grid and are plotted in Fig. 7. For clarity, the magnitude of each color bar was chosen differently because the magnitudes strongly decreased for higher harmonics. The displacements at the fundamental frequency mostly contained the flexural mode in the same manner as in the previous measurements [10], and the displacements at f_0 were four times as large as those of the first harmonic f_1 which contained the torsional modes. At the second harmonic f_2, large magnitudes appeared at the reed's side tips, which was also the torsional mode. Complex displacement patterns were observed only in the higher-frequency harmonics, such as f_4, f_6, and f_8, and their magnitudes were much smaller than the displacements of the fundamental frequency.

The time variation of pressure distributions on the reed for one cycle is shown in Fig. 8. The pressure values are calculated as the difference between the lower and upper surfaces of the reed. The pressure distributions on the reed surface were almost uniform at $t/T = 0.3$ when the reed was closed. Once the reed started open, the tip of the reed had stronger pressure than the middle probably because large velocity of airflow passed on the upper reed surface. It should be noted that there were no complex patterns like the torsional modes of the reed in the pressure distributions. This suggests that the torsional modes were mainly caused by the reed material's oscillation modes and the contact with the edges of the mouthpiece.

3.3. Comparison of flow and sound

The far-field sound spectra calculated for the 1D and 2D reed simulations are shown in Fig. 9(a). Supplemental audio files of these simulations are attached for the reader's information [27]. Overall, the fundamental and odd-number harmonic amplitudes were larger in the low-frequency range ($f/f_0 < 5$), suggesting the typical acoustic characteristics of clarinets [28]. The amplitudes of the harmonics decreased

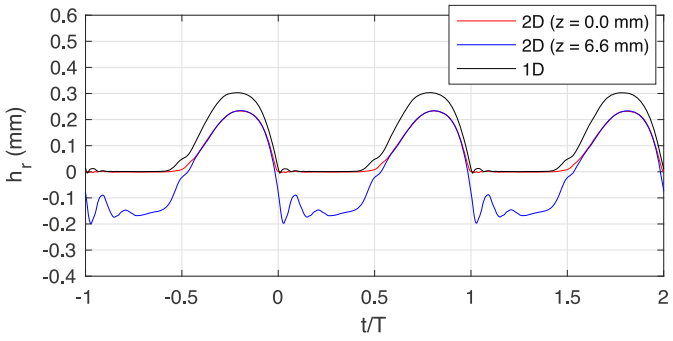

Fig. 6. Reed opening $\boldsymbol{h_r}$ at the middle of the reed $x = 6.7$ mm of the 1D and 2D reed models.

with increasing frequency, and large differences between the 1D and 2D models were observed for $f/f_0 = 9$–10. Moreover, the amplitudes of odd-number harmonics above $f/f_0 = 13$ in the 1D model were larger than those in the 2D model. Consequently, the spectral centroids of the sounds calculated up to $f/f_0 = 25$ for the 1D and 2D reeds were 646 and 521 Hz, respectively. The differences in sound pressure levels (SPLs) between the 1D and 2D models are plotted in Fig. 9(b). The maximum difference reached over 17 dB at $f/f_0 = 9$, and these changes in the supplemental audio were recognizable on the authors' audio devices.

The pressure and volume flow rate at the cross-section inside the mouthpiece, $x = 40$ mm, are plotted in Fig. 10. The pressure was sampled at the center of the y-z cross-section inside the mouthpiece. The pressure of the 1D model was smaller at $0.11 < t/T < 0.27$ and larger at $0.63 < t/T < 0.81$ compared with the pressure of the 2D model. As a result, increases and decreases of the flow rate into the mouthpiece in the 2D model were slightly delayed from the 1D model: a slope at $t/T = 0.39$ was shifted to 0.40 and a slope at $t/T = 0.84$ was shifted to 0.85. In addition, a small peak of flow rate waveform appeared at $t/T = 0.47$ only in the 1D model. These differences in the flow rate were caused by the delay in the reed opening at the middle ($x = 6.7$ mm), as observed in Fig. 6. When the reed was closed, the pressure bounced back from the resonator, causing a reverse flow from the resonator to the mouthpiece. The timing of the beginning of the reverse flow was the same for the 1D and 2D models ($t/T = 0.43$). However, because the 1D reed started opening earlier, as shown in Fig. 6, the flow rate in the 1D model increased earlier than that in the 2D model ($t/T = 0.47$). In contrast, although the center of the 2D reed started opening at the same time as that in the 1D model, the side edges of the reed ($x = 6.7$ mm) did not open simultaneously, and the peaks of the flow rate and pressure appeared later than those in the 1D model. The flow rate waveforms immediately after closing ($t/T = 0.07$) also differed between the 1D and 2D models, presumably because of the rebounding at the reed center due to sudden reed closure (see $t/T = 0.1$ in Fig. 6), which was also observed by [9].

To explore the cause of the far-field sound differences, the magnitude of the sound sources at the mouthpiece was estimated by calculating time derivatives of the flow rate $\partial U/\partial t$ in the same way as [16]. The time variation of $\partial U/\partial t$ for one cycle is plotted in Fig. 11. After the reed closure at $t/T = 0$, small fluctuations of $\partial U/\partial t$ appeared up until $t/T = 0.35$ in the closed phase for both cases. A significant difference was observed at $t/T = 0.45$, where the peak width $t/T = 0.39$–0.48 of the 1D model was increased to $t/T = 0.40$–0.53 in the 2D model.

The magnitudes of $\partial U/\partial t$ at the fundamental frequency f_0 and its harmonics were calculated by DFT and are plotted in Fig. 12. While the discrepancies between the 1D and 2D models were less than approximately 7 dB from $f/f_0 = 1$ to 8, the discrepancy significantly increased to 15 dB at $f/f_0 = 9$ and 18 dB at $f/f_0 = 10$. This result shows the same tendency as the far-field sound pressure levels shown in Fig. 9, indicating that the decrease in sound amplitudes from $f/f_0 = 9$ to 10 due to the 2D reed oscillation was caused by changes in the time variation of the flow rate inside the mouthpiece. The magnitudes of $\partial U/\partial t$ of the 1D model at the higher harmonics ($f/f_0 = 13$ to 19) were larger than those of the 2D model, which were also consistent with the far-field sound characteristics.

4. Discussion

The displacement distributions of the 2D reed model demonstrated that the 2D reed oscillations mainly comprised the first flexural mode, which is same as the previous measurements [10]. This result supports the agreement in sound amplitudes between the simulation of the 1D reed model and the experiment in a previous study in the lower frequency range [16]. In the 2D reed model, the center of the reed was concaved inward by approximately 0.19 mm, and torsional modes appeared at higher frequencies. These changes in the displacement from 1D to 2D altered the waveform of the flow rate in the mouthpiece and

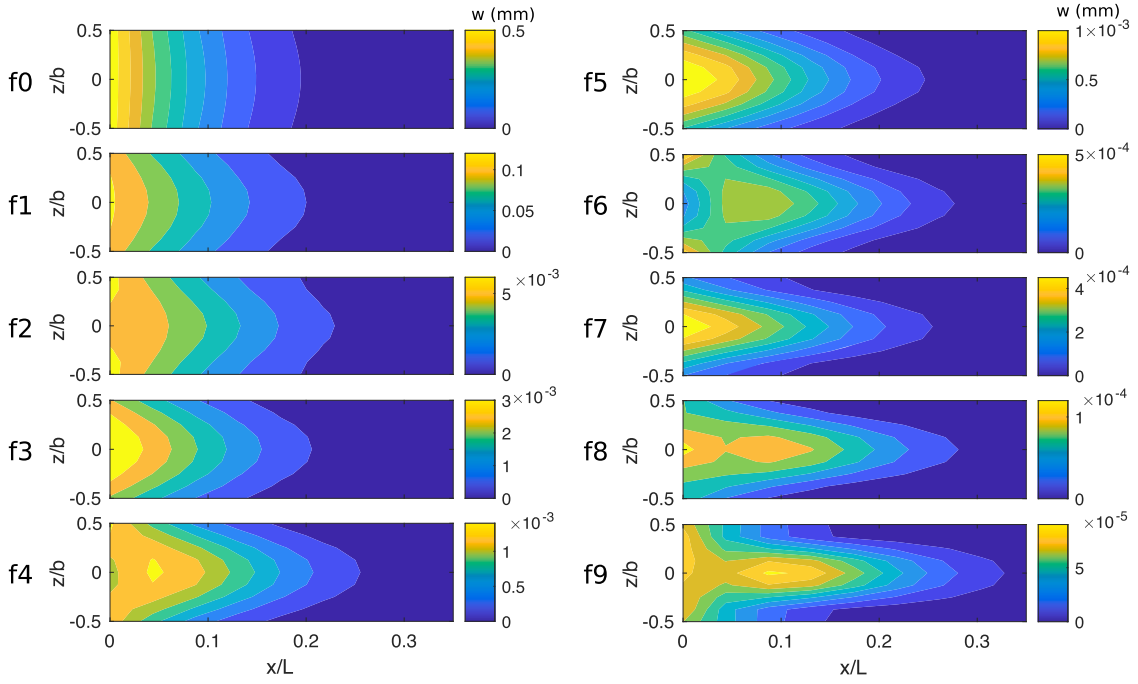

Fig. 7. Displacement magnitudes at fundamental frequency f_0 and its harmonics f_1 to f_9 for 2D reed model. Axes x and z were normalized by the total length $L = 34$ mm and width $b = 13$ mm of the reed.

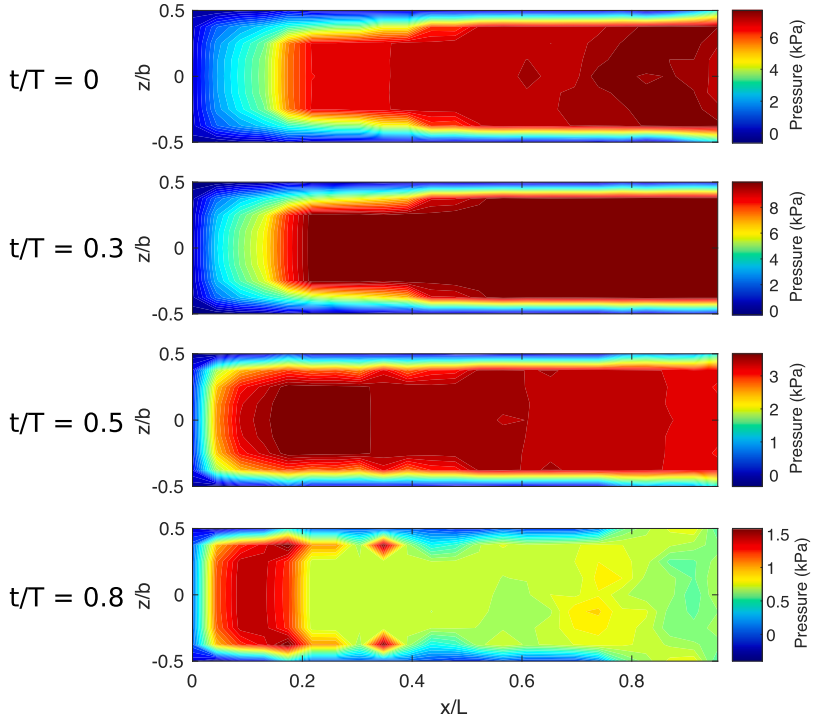

Fig. 8. Time variation of pressure distribution on the reed in one cycle. Axes x and z were normalized by the total length $L = 34$ mm and width $b = 13$ mm of the reed.

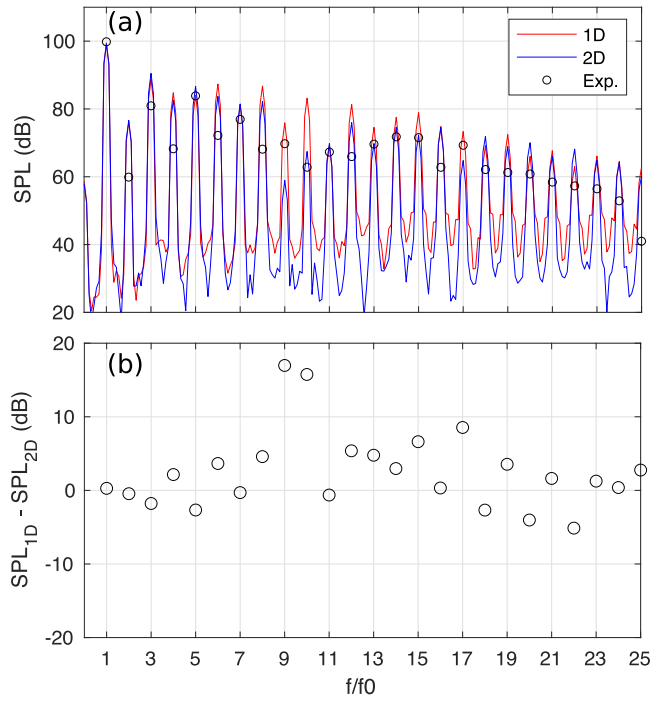

Fig. 9. Spectra of sounds sampled at 100 mm from the resonator for 1D and 2D reed models. (a) Original spectral amplitudes; (b) difference of the amplitudes at the fundamental and its harmonics between 1D and 2D models.

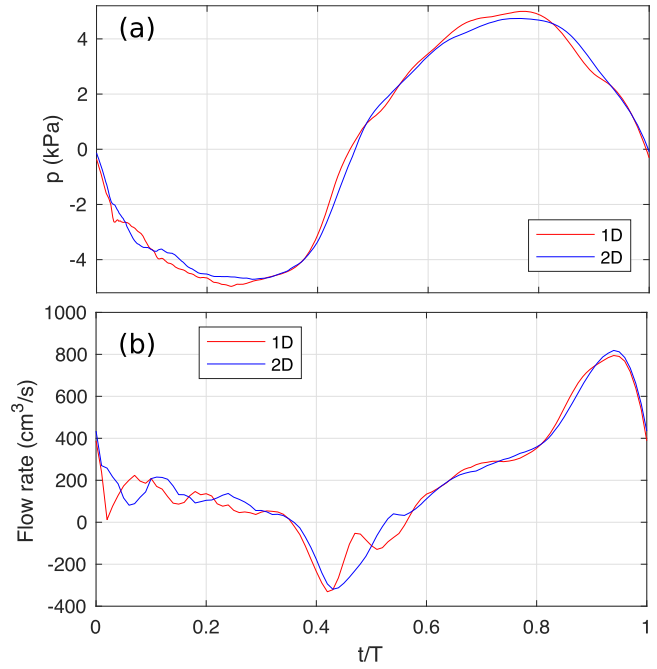

Fig. 10. Pressure (a) and volume flow rate (b) waveforms at $x = 40$ mm inside the mouthpiece for one cycle. Pressure was sampled at the center of the y-z mouthpiece cross-section.

influenced the timbre, mainly at higher frequencies over the 8th harmonic. The harmonic of $f/f_0 = 10$ corresponds to the duration of $t/T = 0.1$, and this indicates that the difference in the peak widths of $\partial U/\partial t$ at $t/T = 0.45$ (i.e., at the timing of the initial reed opening phase) had a significant effect on the far-field sound at around $f/f_0 = 10$. In other words, the later opening of the 2D reeds at the side of the mouthpiece resulted in smaller sound amplitudes at $f/f_0 = 9$–10 compared to the 1D reed model. In addition, the decrease of the sound amplitudes above f/f_0

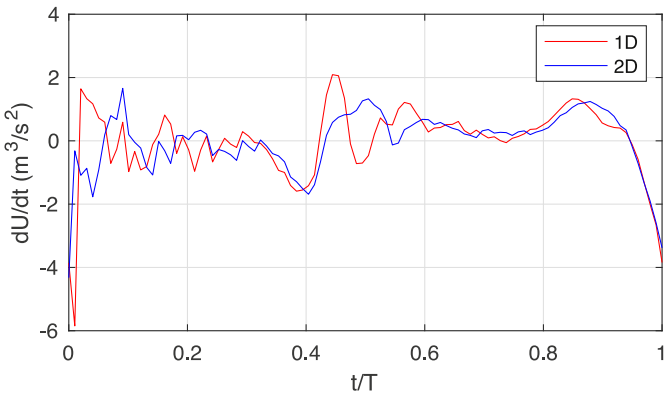

Fig. 11. Time derivative of volume flow rate $\partial U/\partial t$ at $x = 40$ mm inside the mouthpiece for one cycle.

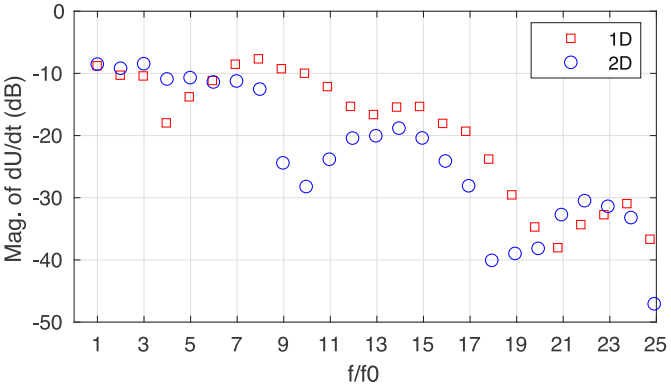

Fig. 12. Magnitudes of time derivatives of flow rates $\partial U/\partial t$ at fundamental frequency and its harmonics.

$= 13$ in the 2D model was probably due to the difference in high-frequency fluctuations of $\partial U/\partial t$ at the closed phase ($0 < t/T < 0.35$), which were also induced by the torsional modes. It should be noted that a rapid decrease in the SPL at $f/f_0 = 9$ in the 2D model was not observed in the experiment, suggesting that the 2D model may have overestimated the torsional mode of reed deformation.

One limitation of this study is that variations in plate thickness in the z-direction were not considered in the 2D reed model. The 2D model assumed a constant reed thickness in the z-direction for comparison with the 1D model, whereas the actual reed was slightly thicker at the center. Although there was no material anisotropy in the experimental reed because a plastic reed was used in the artificial blower, the differences in lateral thickness might have affected the reed deformation as well as the flow rate from the side faces of the mouthpiece. The shapes of the two corner tips, which are rounded in the experiment, also probably affect the vibration characteristics. Improvements in these factors may further increase the accuracy of the far-field sound for the 2D reed model.

Nevertheless, the current simulation demonstrated that 2D reed deformation affects the airflow and sound generation in the clarinet mouthpiece in the high-frequency range, and the proposed methodology enabled the observation of detailed changes in the flow and sound owing to the reed deformation characteristics. Through the comparison between the 1D and 2D reed models under the almost same tip opening waveforms, we found that the difference of side openings between the reed and mouthpiece due to the 2D torsional modes affects the hearable sound characteristics.

Because the effects of anisotropy in actual reeds are known to differ depending on the individual reed [7], these changes in the 2D oscillatory characteristics should also be modeled with plate theory by changing the Young's modulus and Poisson's ratio in each axis, as in [19]. Our next

step will be to model the material anisotropy and individual characteristics of reeds to investigate changes in the timbre of the single-reed instrument.

5. Conclusion

In this study, the effects of 2D reed oscillations on airflow and sound generation in a single-reed instrument were investigated using aeroacoustic simulations coupled with 1D and 2D reed deformation models. The 2D reed model in the self-sustained oscillation deformed mainly in the flexural mode, which was consistent with previous experimental observations. The torsional modes were observed only at higher harmonics. A comparison between the 1D and 2D reed models demonstrated that the 2D reed opened later at the side face of the mouthpiece than the 1D reed, owing to the torsional mode, and the flow rate passing through the mouthpiece was affected, resulting in a significant decrease in the far-field sound amplitudes at $f/f_0 = 9$–10. In addition, the torsional modes of the 2D reed at higher frequencies decreased the sound amplitude above $f/f_0 = 13$, which led to a decrease in the spectral centroid. These results demonstrate the importance of the high-frequency torsional deformation characteristics of reeds on the timbre of single-reed instruments. Moreover, the results suggest the necessity for modeling the material anisotropy and individual characteristics of reeds in future work, which will contribute to the improvement of the assessment for the playability of reed materials and mouthpiece geometry.

CRediT authorship contribution statement

Tsukasa Yoshinaga: Writing – original draft, Software, Investigation, Conceptualization. **Reo Baba:** Writing – review & editing, Validation, Methodology, Investigation. **Hiroshi Yokoyama:** Writing – review & editing, Software, Conceptualization. **Tetsuro Shoji:** Writing – review & editing, Validation, Methodology. **Akira Miki:** Writing – review & editing, Validation, Methodology. **Akiyoshi Iida:** Writing – review & editing, Project administration.

Declaration of competing interest

The authors declare that they have no known competing financial interests or personal relationships that could have appeared to influence the work reported in this paper.

Acknowledgments

This study was partly supported by JSPS KAKENHI (JP23K17195). This work used the computational resources of the Fugaku supercomputer provided by the RIKEN Center for Computational Science through the HPCI System Research Project (Project ID: hp230032). We acknowledge K. Arimoto of the Yamaha Corporation for his helpful comments and discussions.

Supplementary materials

Supplementary material associated with this article can be found, in the online version, at doi:10.1016/j.compfluid.2024.106452.

Appendix A. Effects of lip damping

The effects of lip damping in the numerical setup were investigated using the 2D reed model. The reed-tip opening waveforms under different lip-damping conditions are shown in Fig. A1. By increasing the damping γ only at the lip part slightly decreased the maximum lip opening from 0.49 to 0.46 mm. Other than that, no significant changes were observed in the waveforms, oscillation frequencies, or opening phases.

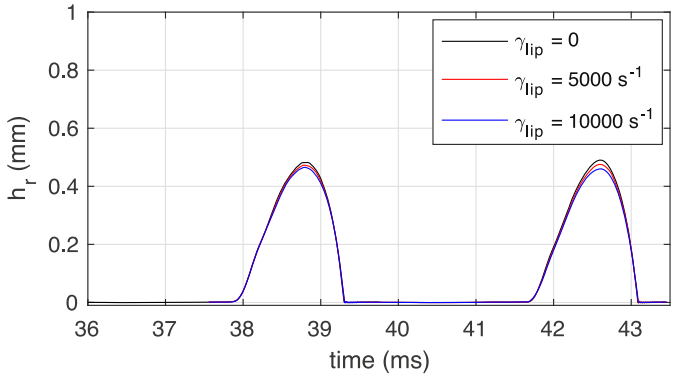

Fig. A1. Reed tip opening simulated with 2D reed model under different lip damping.

Appendix B. frame rates of high-speed camera

To confirm the measurement accuracy of the reed tip displacement using high-speed camera recordings, we compared the tip displacements measured at 6400 and 30,000 fps in Fig. B1. Although slight differences (below $h_r/h_{max} = 0.1$) were observed during the opening and closing phases, the maximum opening timing and overall reed tip waveforms at 6400 fps were consistent with the higher frame rate.

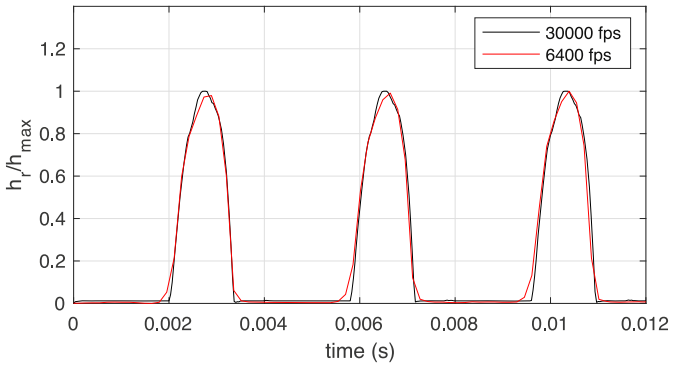

Fig. B1. Reed tip opening measured by high-speed camera with 6400 and 30,000 fps. Tip opening is normalized by the maximum reed opening h_{max}.

Data availability

The data supporting the findings of this study are available from the corresponding author upon reasonable request.

References

[1] Backus J. Vibrations of the reed and the air column in the clarinet. J Acoust Soc Am 1961;33(6):806–9.
[2] Sommerfeldt SD, Strong WJ. Simulation of a player–clarinet system. J Acoust Soc Am 1988;83(5):1908–18.
[3] Idogawa T, Kobata T, Komuro K, Iwaki M. Nonlinear vibrations in the air column of a clarinet artificially blown. J Acoust Soc Am 1993;93(1):540–51.
[4] Almeida A, George D, Smith J, Wolfe J. The clarinet: how blowing pressure, lip force, lip position and reed "hardness" affect pitch, sound level, and spectrum. J Acoust Soc Am 2013;134(3):2247–55.
[5] Chatziioannou V, Schmutzhard S, Pàmies-Vilà M, Hofmann A. Investigating clarinet articulation using a physical model and an artificial blowing machine. Acta Acust United Acust 2019;105(4):682–94.
[6] Campbell DM. Nonlinear dynamics of musical reed and brass wind instruments. Contemp Phys 1999;40(6):415–31.
[7] Pinard F, Laine B, Vach H. Musical quality assessment of clarinet reeds using optical holography. J Acoust Soc Am 2003;113(3):1736–42.
[8] Taillard PA, Laloë F, Gross M, Dalmont JP, Kergomard J. Statistical estimation of mechanical parameters of clarinet reeds using experimental and numerical approaches. Acta Acust. United Acust. 2014;100(3):555–73.
[9] Picart P, Leval J, Piquet F, Boileau JP, Guimezanes T, Dalmont JP. Study of the Mechanical Behaviour of a Clarinet Reed Under Forced and Auto-oscillations With Digital Fresnel Holography. Strain 2010;46(1):89–100.
[10] Ukshini E, Dirckx JJ. Three-dimensional vibration patterns of alto saxophone reeds measured on different mouthpieces under mimicked realistic playing conditions. J Acoust Soc Am 2021;150(5):3730–46.
[11] da Silva RA, Scavone GP, van Walstijn M. Numerical simulations of fluid-structure interactions in single-reed mouthpieces. J Acoust Soc Am 2007;122(3):1798–809.
[12] Shi Y. A numerical framework for fluid-acoustic-structure interaction in clarinet-like instruments. Ph.D. thesis. Quebec, Canada: McGill University Montreal; 2016.
[13] Wang S, Scavone GP. Computational aeroacoustic modeling of single-reed mouthpiece using Palabos. In: Proceedings of the International Symposium on Musical Acoustics 2019; 2019. p. 246–53.
[14] Yokoyama H, Kobayashi M, Iida A. Analysis of flow and acoustic radiation in reed instruments by compressible flow simulation. Acoust. Sci. Tech. 2020;41(5):739–50.
[15] Giordano N, Thacker JW. Navier-stokes-based model of the clarinet. J Acoust Soc Am 2020;148(6):3827–35.
[16] Yoshinaga T, Yokoyama H, Shoji T, Miki A, Iida A. Global numerical simulation of fluid-structure-acoustic interaction in a single-reed instrument. J Acoust Soc Am 2021;149(3):1623–32.
[17] Avanzini F, Van Walstijn M. Modelling the mechanical response of the reed-mouthpiece-lip system of a clarinet. Part I. A one-dimensional distributed model. Acta Acust. United Acust. 2004;90(3):537–47.
[18] Chatziioannou V, van Walstijn M. Reed vibration modelling for woodwind instruments using a two-dimensional finite difference method approach. In: Proceedings of International Symposium on Musical Acoustics (ISMA2007); 2007.
[19] Chatziioannou V. Forward and inverse modelling of single-reed woodwind instruments with application to digital sound synthesis. Belfast: Queen's University; 2011.
[20] Lele SK. Compact finite difference schemes with spectral-like resolution. J Comput Phys 1992;103:16–42.
[21] Liu Q, Vasilyev OV. A Brinkman penalization method for compressible flows in complex geometries. J Comput Phys 2007;227(2):946–66.
[22] Gaitonde DV, Visbal MR. Pade-type higher-order boundary filters for the Navier–Stokes equations. AIAA J 2000;38(11):2103–12.
[23] Leissa AW. Vibration of plates. Washington D.C.: U.S. Government Printing Office; 1969 (NASA SP-160).
[24] Daicel Corporation (2023). "Technical report for cellulose fiber reinforced plastic Celblen series C," available at https://data.novacel.co.jp/pdf/properties/TI-DataSheet-PBG150-Ver0J_NV.pdf (in Japanese, last viewed Oct 18, 2024).
[25] Ogawa T. Introduction to polymeric materials for engineers (in japanese). Tokyo: KYORITSU SHUPPAN CO., LTD.; 1993. p. 44.
[26] McIntyre ME, Woodhouse J. On measuring the elastic and damping constants of orthotropic sheet materials. Acta Metallurgica 1988;36(6):1397–416.
[27] See supplementary material for the audio files synthesized from the simulations of 1D reed (audio1.wav) and 2D reed (audio2.wav) models.
[28] Fletcher NH, Rossing TD. The physics of musical instruments. New York: Springer; 2012.